Nonlinear electron transport in an electron-hole plasma

P. Bowlan,[1] W. Kuehn,[1] K. Reimann,[1] M. Woerner,[1] T. Elsaesser,[1] R. Hey,[2] and C. Flytzanis[3]

[1]*Max-Born-Institut für Nichtlineare Optik und Kurzzeitspektroskopie, 12489 Berlin, Germany*
[2]*Paul-Drude-Institut für Festkörperelektronik, 10117 Berlin, Germany*
[3]*Laboratoire Pierre Aigrain, École Normale Supérieure, 75231 Paris, France*

Charge transport in an electron-hole plasma driven by high-field terahertz (THz) pulses is strongly influenced by electron-hole interactions, as has been shown in a recent publication [P. Bowlan *et al.*, Phys. Rev. Lett. **107**, 256602 (2011)]. We introduce a picture of high-field THz transport which accounts for the roles of both types of carriers including their interactions. While holes make a negligible contribution to the current, they are heated by absorbing energy from the driving THz field and introduce a friction force for the electrons over a period of about 500 fs. Our model uses an extended version of the loss-function concept to calculate the time-dependent friction. The local field that drives the electrons differs from the incident THz field by screening due to Coulomb correlations in the plasma. We illustrate how spatial correlations between charged particles (electrons, holes, impurities) create a significant local-field correction to the THz driving field. The dominant contribution stems from Coulomb-correlated heavy-hole wave packets, which are strongly polarizable via inter-valence-band transitions.

PACS number(s): 72.20.Ht, 72.80.Ey, 78.47.J−

I. INTRODUCTION

Intense femtosecond terahertz (THz) pulses allow for driving carrier transport in semiconductors at very high carrier velocities and provide a time resolution below typical scattering times.[1] New phenomena have been discovered in this regime, among them partial Bloch oscillations in a bulk semiconductor and the undressing of polarons.[2–4] The conventional theoretical framework for describing charge transport such as the semiclassical Boltzmann transport equation is often insufficient to explain high-field transport phenomena on ultrafast time scales.[5] "High field" in this context means that the (frequency-dependent) conductivity deviates from its value at low field. The field strength for this to happen depends on the material and on the time scale investigated. As an example, in GaAs at room temperature the drift velocity in a static field deviates from a linear field dependence for fields above 3 kV/cm.[6]

The failure of the semiclassical Boltzmann transport equation on ultrafast time scales is mainly due to the fact that scattering takes a finite time to happen. For example, if the dominant scattering process is with optical phonons, this can not happen faster than the inverse of the highest phonon frequency ($\nu_{LO}^{-1} = 120$ fs in GaAs) in the respective material.[2] Therefore, at very early times after turning on the driving field, the carrier motion is essentially ballistic, i.e., not influenced by scattering, and the velocity can be considerably higher than the steady-state value.[3] Such behavior has been observed in experiments in which a 10-fs infrared pulse injected electron-hole pairs into a semiconductor layer to which a high static electric field was applied.[7–9] For high enough driving fields $E(t) > 50$ kV/cm, the transport can be ballistic for times even longer than ν_{LO}^{-1} because the electrons move faster than the lattice responds, leading to a decoupling of electrons and phonons. Using driving fields between 50 and 300 kV/cm, electron transport in GaAs was recently shown to be perfectly ballistic over the entire duration of the driving

THz pulse of 1.5 ps.[3] The absence of scattering is manifested in the observation of partial Bloch oscillations in a bulk crystal.

The existing results on high-field THz transport (for a review, see Ref. 1) provide very limited insight into the behavior of photoexcited electron-hole plasma and the particular roles of the two types of carriers. To address this issue, we recently studied high-field transport of an electron-hole plasma in bulk GaAs and demonstrated the occurrence of a time-dependent frictional force which originates from electron-hole interactions.[10]

To analyze this behavior theoretically, we introduced a theoretical model based on the concept of wave packets. Motivated by the periodicity of a crystal, the standard description of electrons, phonons, and other quasiparticles in solid-state theory uses infinitely extended plane waves. These plane waves are extremely unstable against decoherence.[11–13] Even very small perturbations lead to a very fast localization. In contrast, wave packets are much more stable against decoherence. The wave packet size is determined by the amount of decoherence, which is in turn determined by the temperature. Although it is possible to describe a wave packet as a coherent superposition of plane waves, it turns out that it is simpler to directly use wave packets. They can be labeled by the position, momentum, and wave-packet size, either in real or in momentum space. In this way, one has in a first approximation the classical equations of motion according to Ehrenfest's theorem. The force acting on a wave packet averages over the short-wavelength potential fluctuations underneath such a wave packet, leading to a strongly reduced "effective" interaction with short-wavelength quasiparticles. On the next higher level of approximation, one has to take into account the change of the wave-packet size caused by the interactions with other particles. Even higher approximations, which we do not consider in the following, would lead to a time-dependent change of the shape of the wave packet.

In this paper, we present the wave-packet treatment of high-field carrier transport in full detail. The theoretical results

are complemented by additional experimental data to address the following questions: (i) Does the transition from ballistic to driftlike transport of electrons in an electron-hole plasma depend on the THz frequency? (ii) Does the high-field electron transport on ultrafast time scales depend on the delay τ between the photoexcitation of electron-hole pairs and the THz pulse driving the electrons? (iii) Is the electron transport influenced by the initial excess energy of the photoexcited electron-hole pairs? The paper is organized as follows. The theoretical model and its results are presented in Sec. II, followed by a summary of the additional data in Sec. III. A discussion is presented in Sec. IV, followed by conclusions in Sec. V.

II. THEORY

For decades, high-field carrier transport in semiconductors has been the subject of extensive theoretical literature.[6,14–24] In this context, the semiclassical Boltzmann transport equation is probably the most widespread concept.[6,25] In most cases, the scattering terms of the Boltzmann equation are calculated by perturbation theory, inherently assuming that the duration of scattering events is short compared to the time interval between them. This assumption breaks down on ultrafast time scales (i.e., $t < 300$ fs) and, thus, the Boltzmann transport equation fails and predicts wrong scenarios of high-field transport.[2,3,5] Two reasons are responsible for this: (i) The semiclassical Boltzmann transport equation can not account for quantum-kinetic memory effects in the electron-phonon interaction. Theoretical results[14,15] for $E < 80$ kV/cm have shown that energy nonconserving transitions lead to interferences between the electron–electric-field and the electron-phonon interaction allowing ballistic transport on ultrafast time scales. (ii) In the semiclassical Boltzmann transport equation, the state of a charge carrier is described by its momentum $\vec{p} = \hbar\vec{k}$ and by its spatial position $\vec{r}$, both being interpreted in a "classical" picture.[6] Quantum mechanics, however, does not allow for a precise, simultaneous measurement of both quantities ($\Delta x^2 \Delta p_x^2 \geqslant \hbar^2/4$), leading in a natural way to the concept of wave packets. Recently, we developed a dynamic polaron model that correctly incorporates both issues.[2,3,5] In the following, we describe an extension of this model for photoexcited electron-hole plasmas in semiconductors.

A. Transient friction force derived from the loss-function concept

The energy loss of charged particles in a solid can be described by the imaginary part of the inverse dielectric function $\epsilon(q,\omega)$. If a (classical) particle of charge e and velocity $\vec{v}$ enters a crystal, the dielectric displacement is

$$\vec{D}(\vec{r},t) = -\nabla \frac{e}{|\vec{r} - \vec{v}t|}. \tag{1}$$

Quantum mechanically, this equation is an approximation valid if the wave-packet size of the particle is smaller than the interatomic distance in the solid, which is the case, e.g., for electrons with keV kinetic energies. Otherwise, the δ-like charge density on the right-hand side of Eq. (1) has to be convoluted with the actual charge density of the wave packet. In the following, we consider spherically symmetric Gaussian

wave packets with a spatial extent (root mean square) of $\sqrt{\Delta x^2}$. With such a charge distribution, the previous equation reads as

$$\vec{D}(\vec{r},t) = -\nabla \left[\int \frac{\exp\left(-\frac{|\vec{r}-\vec{r}'|^2}{\Delta x^2}\right)}{(\pi \Delta x^2)^{3/2}} \frac{e}{|\vec{r}' - \vec{v}t|} d^3\vec{r}' \right]. \tag{2}$$

The semiclassical friction force acting on the charged particle when propagating through a medium with the dielectric function[26] $\epsilon(q,\omega)$ is given by the electric field created by the medium acting at the spatial position of the particle $\vec{E}(\vec{r} = \vec{v}t,t)$:

$$\vec{\tilde{E}}(\vec{q},\omega) = \frac{\vec{\tilde{D}}(\vec{q},\omega)}{\epsilon_0} \left[\frac{1}{\epsilon(q,\omega)} - \frac{1}{\epsilon(q,\infty)} \right]. \tag{3}$$

$\vec{\tilde{E}}(\vec{q},\omega)$ and $\vec{\tilde{D}}(\vec{q},\omega)$ are the four-dimensional Fourier transforms of $\vec{E}(\vec{r},t)$ and $\vec{D}(\vec{r},t)$, respectively. The second term in Eq. (3) subtracts the field from the carrier itself. In the quantum mechanical version of Eq. (3) [cf. Eq. (57) of Ref. 27], one has to consider the energy and momentum conservation of the quanta of the elementary excitations contained in $\epsilon(q,\omega)$. Additionally, one also has to consider the thermal fluctuations of the elementary excitations. For the energy relaxation rate and the total scattering rate, this has been done in Refs. 28–30.

The frequency- and wave-vector-dependent dielectric function $\epsilon(\omega,q)$ consists[28–31] of the high-frequency background due to bound electrons (ϵ_∞), the lattice contribution $[\chi_L(\omega)]$, and contributions from the free electrons and holes. Since both heavy- and light-hole bands are involved, also inter-valence-band contributions to $\epsilon(\omega,q)$ have to be included.

In THz-driven electron-hole plasmas, there are two mechanisms of light-matter interaction: (i) the acceleration of carriers, and (ii) the absorption via inter-valence-band transitions. In our experiments, holes make only a minor contribution to the current, so that in the following we take $v_h = 0$. The electron ensemble is characterized by an average wave vector $k \neq 0$ and a width $\sqrt{\Delta k^2}$, resulting in a separation of the electron and hole ensembles in k space. In a parabolic band, k is proportional to the current and Δk^2 determines its dynamics. In the ballistic limit, $k \gg \sqrt{\Delta k^2}$. In the electron-hole plasma, the scattering between electrons and holes results in an exchange of momentum and energy between the two subensembles. A particularly efficient scattering mechanism is the electron-induced excitation of heavy holes to the light-hole band.[30] Carrier thermalization, i.e., the formation of quasiequilibrium distributions in the spatially separated electron and hole ensembles with a common carrier temperature T_{eh}, occurs on a sub-100 fs time scale[32] and involves electron-electron, electron-hole, as well as intra- and inter-valence-band scattering of holes. It is, thus, justified to describe Δk^2 on the slower time scale of the THz experiment by the common carrier temperature T_{eh}. In this regime, interaction of electrons with holes results in a gradual increase of Δk^2, i.e., an increase of T_{eh}, causing a transition to driftlike transport.

The time dependence of the electron velocity is due to the force from the local electric field acting on the electron and to the friction force, described by the momentum relaxation time

τ_m. This leads to

$$\frac{dv_e}{dt} = -\frac{v_e}{\tau_m(v_e, p, T_{\text{eh}}, T_L)} - \frac{e\, E_{\text{loc}}(t, p, T_{\text{eh}})}{m}. \quad (4)$$

To determine the dependence of τ_m on v_e, p, T_{eh}, and T_L,[33] we extended the concept of Eq. (57) of Ref. [27] to the more general loss-function concept.[28,29] Furthermore, we included the finite size of the electron wave packet [the thermal de Broglie wavelength[3,34] $(\Delta x^2)^{-1} = 4\,\Delta k^2 = 4\,m\,k_B\,T_{\text{eh}}/\hbar$]

$$
\begin{aligned}
\tau_m^{-1} = \frac{e^2}{k^2 \epsilon_0} \int_{-\infty}^{\infty} \int \exp\left(\frac{-\hbar^2 q^2}{4m\, k_B\, T_{\text{eh}}}\right) \frac{\vec{q} \cdot \vec{k}}{q^2\, |\epsilon(\omega, q)|^2} \\
\times \left\{ \frac{\text{Im}[\chi_L(\omega)]}{\exp\left(-\frac{\hbar\omega}{k_B T_L}\right) - 1} + \frac{\text{Im}[\chi_h(\omega, q, T_{\text{eh}})]}{\exp\left(-\frac{\hbar\omega}{k_B T_{\text{eh}}}\right) - 1} \right\} \\
\times \delta\left(\frac{\hbar^2[(\vec{k} + \vec{q})^2 - \vec{k}^2]}{2m} + \hbar\omega\right) d^3\vec{q}\, d\omega. \quad (5)
\end{aligned}
$$

This equation contains the hole susceptibility χ_h but not the electron susceptibility, since electron-electron scattering can not change the total momentum of the electron ensemble[35] and, thus, can not lead to friction.

The energy deposited in the sample via THz absorption heats the carrier system and yields a time-dependent carrier temperature $T_{\text{eh}}(t)$:

$$\frac{3}{2} k_B[T_{\text{eh}}(t) - T_L] = \frac{-e\, n}{n + p} \int_{-\infty}^{t} v_e(t') E_{\text{dr}}(t')\, dt' - \frac{m\, v_e^2(t)}{2}. \quad (6)$$

$T_{\text{eh}}(t)$ is given by the total deposited energy minus the kinetic energy of the electrons undergoing transport. We have neglected here electron cooling since this occurs on longer times not relevant to our experiments. The energy left in the carrier system after the end of the THz pulse is very small for the n- and p-type samples, pointing to small THz absorption and minor changes of T_{eh}, while carrier temperatures higher than 4000 K are found for the photoexcited samples.

In Fig. 1, the resulting friction for electrons in GaAs is plotted as a function of electron wave vector and compared to the friction for the initial $T_{\text{eh}} = 300$ K. With only electrons present at $T_{\text{eh}} = 300$ K (solid black line), friction at small k vectors is due to the absorption of LO phonons. The strong enhancement of the momentum relaxation rate around $k = 2.5 \times 10^6$ cm^{-1} is caused by the onset of LO phonon emission, which now dominates momentum relaxation. With increasing k, the momentum changes by LO phonon emission and absorption tend to compensate each other, resulting in a decrease of the relaxation rate from its maximum value. The addition of holes opens up new channels of electron-hole scattering which enhance the momentum relaxation rate throughout the k range shown. Here, electron-induced transitions of heavy holes to the light-hole valence band make a strong contribution.[30] For a high carrier temperature $T_{\text{eh}} = 5000$ K, both carrier-carrier and carrier-phonon scattering are enhanced, giving rise to substantially higher rates of momentum relaxation. The concomitant strong enhancement of friction results in the transition from ballistic to driftlike transport as shown in Figs. 1 and 2 of Ref. [10].
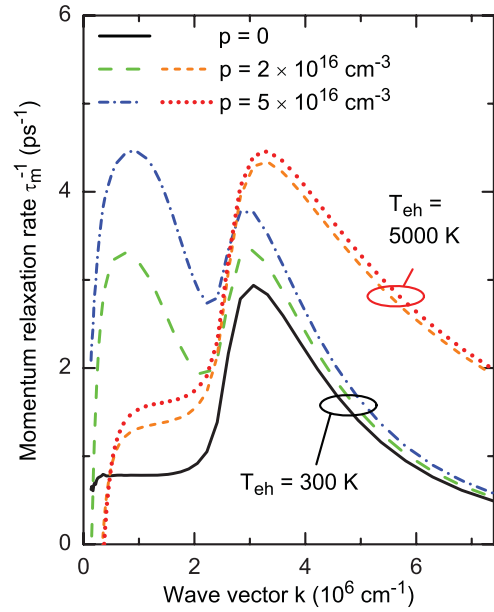

FIG. 1. (Color online) Calculated momentum relaxation rates τ_m^{-1} in GaAs of an electron in the Γ valley as a function of its wave vector k for hole densities p and carrier temperatures T_{eh} as indicated.

B. Lorentz-Lorenz correction to the local driving field in an electron-hole plasma

A surprising experimental finding of our work is that spatial correlations between charged particles (electrons, holes, impurities) can create a significant local-field correction to the THz driving field. Starting at room temperature, a hole density as low as $p \approx 5 \times 10^{16}$ cm^{-3} leads to a local-field correction that halves the THz driving field. Gradual heating of the carrier gas during interaction with the THz field diminishes the Coulomb correlation of heavy holes, leading to a vanishing local-field correction at late times. In the following, we present a semiclassical model that illustrates the physics of the local-field correction in detail.

So far, the concept of the Lorentz-Lorenz field has mainly found its application in the physics of electrically insulating materials, e.g., in the local-field correction of the refractive index of dense media.[37–39] For conducting media such as metals or plasmas, local-field corrections according to the Lorentz-Lorenz field concept are typically less important,[40] although many-body theories for the dielectric constant (cf. Sec. 5.5.3 of Ref. [25]) invoke such effects whenever spatial correlation of charges plays a significant role. In the semiclassical model presented here, we explicitly show that the Lorentz-Lorenz field correction is even present in a plasma if (i) it consists of localized charged particles, i.e., quantum mechanical wave packets and (ii) there is a spatial correlation between charges of both the same and opposite signs.

For simplicity, we calculate the Coulomb energy between two electrically charged wave packets (charges Q_1 and Q_2, spatial extension: $\sqrt{\Delta x^2}$, background dielectric constant ϵ_b) at positions $\vec{r}_1$ and $\vec{r}_2$ with the effective potential

$$V(\vec{r}_1, \vec{r}_2, \Delta x^2) = \frac{Q_1 Q_2}{\epsilon_b \epsilon_0 \sqrt{4\Delta x^2 + |\vec{r}_1 - \vec{r}_2|^2}}. \quad (7)$$
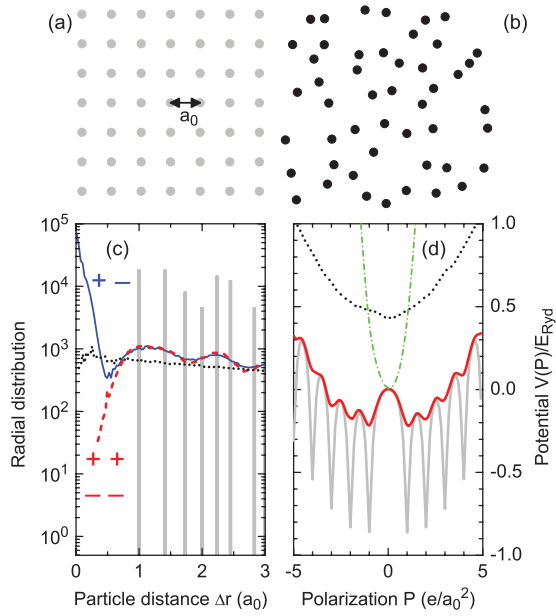
FIG. 2. (Color online) (a) Charges on a square lattice (Ref. 36) with lattice constant a_0. (b) Charges at random positions. (c) Radial distributions of spatially correlated charges (frequency of occurrence vs particle distance). Gray lines: charges on a simple cubic lattice, the three-dimensional analog of the case in (a). Dotted line: uncorrelated particles [random positions of charges in space, analog to (b)]. The solid and dashed lines show radial correlations of Coulomb-correlated charges in a plasma at a temperature of $k_B T = E_{\rm Ryd}$ (dashed line: charges of the same sign; solid line: charges of opposite sign). (d) Corresponding many-body Coulomb potentials at the origin of the ellipsoid as a function of the macroscopic polarization P in the ellipsoid, for a random distribution (dotted line), for a cubic lattice (gray line), and for a plasma (solid line), for P parallel to the ellipsoid axis. The dashed-dotted line shows the depolarization field (P perpendicular to the ellipsoid axis), which does not depend on the spatial correlation of the charges.

Such a potential describes correctly the Coulomb interaction at large distances $|\vec{r}_1 - \vec{r}_2| \gg \sqrt{\Delta x^2}$, but avoids its divergence at $|\vec{r}_1 - \vec{r}_2| = 0$. In a semiclassical picture (Ehrenfest's theorem), the divergence is removed by averaging the Coulomb force over the finite size of the involved wave packets. With the spatial extension equal to the Bohr radius, $\sqrt{\Delta x^2} = a_{\rm Bohr}$, one gets the correct ground-state energy of an exciton or a neutral impurity. Next, we place on a simple cubic lattice[36] (lattice constant: $a_0 = p^{-1/3}$ with hole density p) an equal number of positive and negative charges within an ellipsoid of revolution (spheroid).[41] Now, we calculate the potential at the origin of the ellipsoid (at this location no charge was placed) as a function of the spatial separation $\Delta \vec{r}$ between the two arrays consisting of the positive and the negative charges. The results (together with the radial distributions) are shown as gray lines in Fig. 2. For an oblate ellipsoid and $\sqrt{\Delta x^2} \ll a_0$, one gets the expected results: For a spatial separation parallel to the revolution axis, the calculation yields the potential [dashed-dotted line in Fig. 2(d)] of the sum of the Lorentz-Lorenz field plus the depolarization field, i.e., $\vec{E}_{\rm loc} = \frac{1}{3} \vec{P}/(\epsilon_b \epsilon_0) - \vec{P}/(\epsilon_b \epsilon_0) = -\frac{2}{3} \vec{P}/(\epsilon_b \epsilon_0)$ with

the macroscopic polarization $\vec{P} = ep\Delta \vec{r}$. In contrast, for a spatial separation of the charged arrays perpendicular to the revolution axis of the oblate ellipsoid, one gets only the potential of the Lorentz-Lorenz field, i.e., $\vec{E}_{\rm loc} = \frac{1}{3} \vec{P}/(\epsilon_b \epsilon_0)$. So far, our semiclassical many-body model just confirmed the well-known physics contained in the concept of the Lorentz-Lorenz field.[37–39]

Interesting new physics arises when considering deviations from such a perfect insulating crystal. First, we consider the influence of the wave-packet size on the local field. Our calculations show that when we increase the wave-packet size $\sqrt{\Delta x^2}$ toward the next-neighbor distance a_0 of the cubic lattice the Lorentz-Lorenz field gradually diminishes and even vanishes beyond this point. In contrast, the amplitude of the depolarization field does not depend on $\sqrt{\Delta x^2}$, i.e., it even exists for particle wave functions extended over the entire ellipsoid (plane-wave approach).

To investigate the influence of the spatial correlation of charges on the local field, we added various disorders on the spatial positions of the charges. To this end, we introduced random (normally distributed) fluctuations $\Delta \vec{R}$ of various amplitudes $\sqrt{\Delta R^2}$ on both the relative displacement between the positive and negative charges of each pair within the cubic array and on the absolute positions of individual pairs within the array. Similar to the influence of the wave-packet size (see above), once either the fluctuations within a neutral pair or those of the absolute positions of individual pairs reach an amplitude in the order of the next-neighbor distance, i.e., $\sqrt{\Delta R^2} \approx a_0$, the Lorentz-Lorenz field gradually diminishes. In contrast, the depolarization field is unaffected by the disorder. In Fig. 2, we show these trends together with the spatial correlations of the positive and negative charges. To summarize, our semiclassical model calculations show that the Lorentz-Lorenz field occurs only if the wave packets are small compared to the interparticle distance, if a repulsive correlation between charges of identical sign exists and if an attractive correlation between charges of opposite sign exists.

Positively charged heavy holes in the valence band of a semiconductor fulfill such conditions. At room temperature, the wave-packet size is about $\sqrt{\Delta x^2} \approx 1$ nm, much smaller than the average mutual separation between them, $p^{-1/3} \approx 30$ nm for $p \approx 5 \times 10^{16}$ cm^{-3}. On the one hand, due to the mutual Coulomb repulsion, they avoid each other, leading to a pronounced antibunching of heavy holes [dashed line in Fig. 2(c)]. On the other hand, a heavy hole is a polarizable particle on its own, i.e., an external electric field can cause a coherent superposition of a heavy- and light-hole wave packet, the mutual spatial separation of which shows a pronounced attractive spatial correlation, similar to that between the electron and the ion core within an atom. Thus, our surprising experimental finding[10] that, at $T = 300$ K, a hole density as low as $p \approx 5 \times 10^{16}$ cm^{-3} leads to a local-field correction that halves the THz driving field is the consequence of the Lorentz-Lorenz field in a Coulomb-correlated plasma. Heating of the carrier gas during interaction with the high-field THz pulse gradually diminishes the Coulomb correlation of heavy holes, leading to a vanishing local-field correction at late times.

III. EXPERIMENT

Both the applied electric field and the current need to be measured with a time resolution of 100 fs in order to check the predictions of theory by experiment. In our measurements, we use the electric field of a strong THz pulse and determine its time dependence by electro-optic sampling. The time-dependent current leads to the emission of transient electric fields, which can also be measured by electro-optic sampling. If the current is limited to a layer thin compared to the THz wavelength, the relation between the current $j(t)$ and the emitted field $E_{em}(t)$ is particularly simple:[45–47]

$$j(t) = -2E_{em}(t)/(Z_0 d). \tag{8}$$

To measure the emitted field, we use that the transmitted field $E_{tr}(t)$ is equal to the sum of emitted and incident fields $E_{tr}(t) = E_{in}(t) + E_{em}(t)$. Thus, we obtain the emitted field as the difference between the transmitted and incident fields. To extract the current from the photoexcited carriers, we measure the transmitted field transients with and without photoexcitation, $E_{tr}^{with}(t)$ and $E_{tr}^{without}(t)$. The difference between these transients is the field emitted from the photoexcited carriers. The corresponding current is then obtained using Eq. (8). In this thin-layer geometry, the field acting on the carriers, the driving field, is equal to the transmitted field[45–47] $E_{dr}(t) = E_{tr}(t)$.

Our sample is grown by molecular beam epitaxy. It consists of a 500-nm-thick GaAs layer, which clearly fulfills the requirement for the thin-layer geometry since $\lambda_{THz} = 150\ \mu$m, and two 300-nm $Al_{0.4}Ga_{0.6}As$ cladding layers. All experiments shown here were done with the sample at room temperature. Our experimental setup is shown in Fig. 3. The
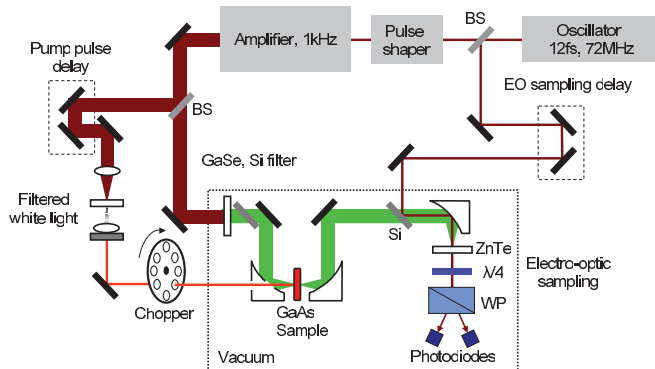

FIG. 3. (Color online) Experimental setup. A Ti:sapphire oscillator-amplifier system generates 30-fs pulses around 800-nm wavelength. THz pulses are generated by optical rectification in GaSe. A Si filter removes the unconverted 800-nm light. The THz pulses are focused onto the GaAs sample and then imaged onto a ZnTe crystal for electro-optic sampling, using a small portion of the unamplified 800-nm pulses as probe. Part of the amplifier pulses is sent to a sapphire plate for a white-light continuum, which is spectrally filtered to vary the wavelength for photoexcitation between 650 and 885 nm. With a chopper synchronized to half the amplifier repetition rate, we measure at every time step the THz pulse through the sample both with and without photoexcitation. The photoexcitation pulse is collinear with the THz pulse, unfocused at the sample, and enters through a small hole in the first parabolic mirror. The entire path of the THz pulse is in vacuum.

THz driving pulses are generated by optical rectification of amplified 800-nm pulses in GaSe.[46] The THz beam is focused onto our sample to accelerate the generated carriers. For electro-optic sampling, we use a thin ZnTe crystal, and the oscillator pulses as the probe pulses. The entire THz beam path is within a vacuum chamber. For photoexcitation, we generate a white-light continuum. By spectral filtering, we can vary the wavelength used for excitation. Additionally, some measurements were done with 400-nm excitation, obtained by second-harmonic generation. Autocorrelation measurements confirmed that the photoexcitation pulses were always shorter than 150 fs, i.e., much shorter than the THz transients. There are two delays in the experiments: the delay between the pump pulse and the THz pulse (hereafter this is called delay) and the electro-optic sampling delay measuring the time dependence of the THz electric field (hereafter this is called time).

In all experiments discussed in the following, we analyzed the measured fields with the method already presented in Ref. 10. We compare the THz transient emitted by the sample with two limiting cases: perfect drift motion and perfect ballistic motion. For perfect drift motion, we have

$$j_{drift}(t) \propto E_{dr}(t) \tag{9}$$

for perfect ballistic transport

$$j_{ballistic}(t) \propto \int_{-\infty}^{t} E_{dr}(t')dt'. \tag{10}$$

For a monochromatic field, this yields a $\pi/2$ phase shift compared to the drift motion. To get a quantitative measure for intermediate cases, we introduce the ballisticity $b(t)$, defined by

$$b(t) = \frac{\arg[\tilde{j}(t)] - \arg[\tilde{j}_{drift}(t)]}{\arg[\tilde{j}_{ballistic}(t)] - \arg[\tilde{j}_{drift}(t)]}, \tag{11}$$

using the definitions in Eqs. (8)–(10). The complex valued $\tilde{j}(t)$ are obtained from the real valued $j(t)$ by a Fourier transform, zeroing the negative-frequency components, multiplying all components with frequencies >0 by 2, and a back transform. The ballisticity defined in Eq. (11) is equal to one for perfect ballistic transport and equal to zero for perfect drift transport.

Before presenting additional results, we want to shortly summarize the results already shown in Ref. 10. (i) If the only type of carriers present are electrons (*n*-type sample, no photoexcitation), the transport is ballistic over the whole length of the THz pulse. (ii) If there are only holes present (*p*-type sample, no photoexcitation), the current for the same carrier density is at least 7.5 times lower and within the noise limit of the experiment. (iii) If both electrons and holes are present, the transport is dominated by the electrons and there is a transition from ballistic transport at the beginning of the THz pulse to drift transport at later times. The higher the hole density, the faster the transition toward drift transport (comparison of photoexcited *n*-type, *p*-type, and undoped samples). Thus, although holes do not contribute appreciably to the current, they influence the electron transport.

We now present results that show the dependence of transport on (i) the THz frequency, (ii) the delay between the excitation pulse and the THz pulse, including the case when carriers are generated during the THz pulse, and (iii) the
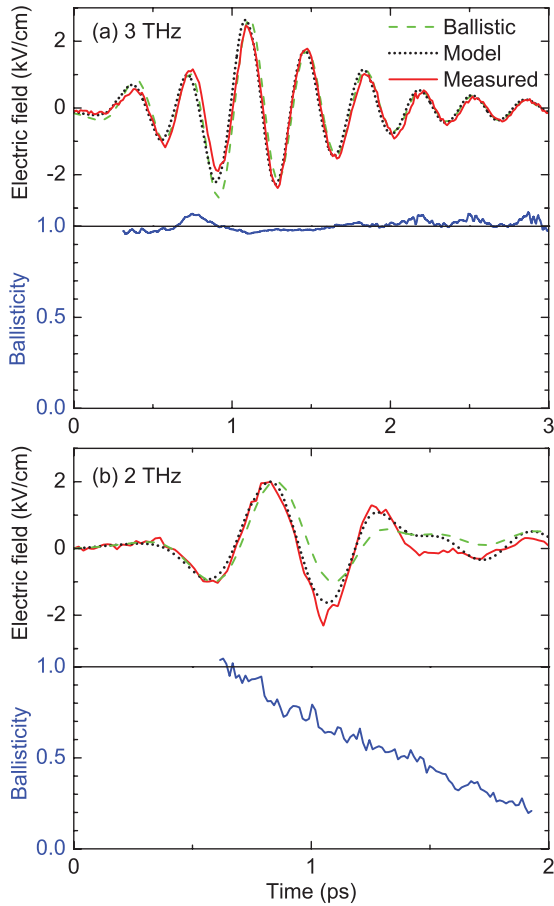
FIG. 4. (Color online) Measured emitted fields (solid lines) using driving fields with center frequencies of (a) 3 and (b) 2 THz. For comparison, we also plot the ballistic responses calculated from Eq. (10), and the fields predicted by our model. The lower parts of both figures show the time dependence of the ballisticity [Eq. (11)].

FIG. 5. (Color online) Transport for small delays between photoexcitation and THz pulses. The measured emitted field amplitude (a) and the ballisticity (b) are plotted versus delay and time. For these measurements, the photoexcitation wavelength was 800 nm, the density 4×10^{16} cm^{-3}, and the THz field amplitude 50 kV/cm. (c), (d) Corresponding results from our model.

excitation wavelength. Using a photoexcitation wavelength of 885 nm, an excitation density of $n = p \approx 2 \times 10^{16}$ cm^{-3}, and a THz field strength of 25 kV/cm, we compared the emitted fields for different THz center frequencies of 3 and 2 THz. These results are shown in Fig. 4. When using a 2-THz driving field, as we do for all further measurements in this paper, we see the transition from ballistic to drift transport, which occurs over $\approx$300 fs as described in Ref. 10. For 3 THz, however, the transport is nearly perfectly ballistic over the entire duration of the driving THz field. This result is reproduced by our model.

To study transport during the time overlap of photoexcitation pulse and THz pulse, we used attenuated pulses from the Ti:sapphire amplifier at 800 nm for photoexcitation to achieve the best possible time resolution and the lowest noise. The experimental results are compared with the results from our model in Fig. 5. At longer delays, when the THz pulse and photoexcitation pulse no longer overlap, the results of the measurement in Fig. 5 are the same as those discussed above and in Ref. 10. As shown in Fig. 5(b), the ballisticity begins with a value of one, indicating perfect ballistic transport, but decreases slowly with time as the transport becomes more driftlike. At shorter delays, when the photoexcitation pulse arrives within the driving THz pulse, oscillations are seen in
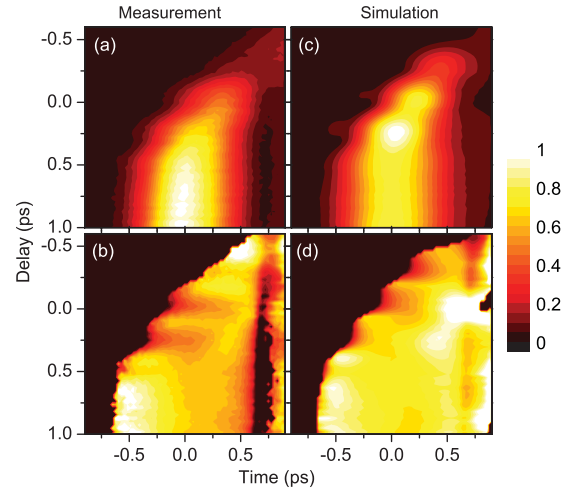
both the emitted field amplitude and in the ballisticity. Figure 6 shows a cut along the center of the photoexcitation pulse, i.e., for $t = -\tau$. The electron motion is more ballistic when the photoelectrons are injected at the driving-field extrema compared to the case when they are injected near the zeros of the driving field.

To see how the electron current varies when the carriers are generated at different k values in the band structure, we photoexcited carriers with various wavelengths (see Table I). The same driving THz pulse (2 THz, 50 kV/cm) and the same excitation densities ($n = p \approx 2 \times 10^{16}$ cm^{-3}) were used in all experiments. Figure 7 shows the emitted fields for delays of 1.5, 15, and 35 ps after excitation. For long delays, the emitted field transients are nearly independent of excitation wavelength, but at short delays we find a decrease of the field amplitude with shorter wavelengths. In Fig. 8, the maximum amplitude of the recorded THz transient is shown as a function of delay. At a photoexcitation wavelength of 885 nm, the amplitude is constant; at shorter wavelengths,
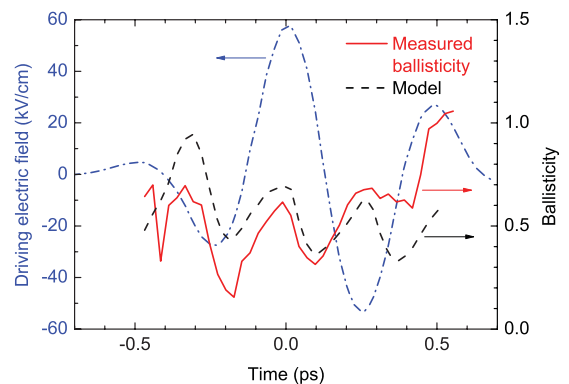

FIG. 6. (Color online) The measured (solid line) and calculated (dashed line) ballisticities along the center of the photoexcitation pulse together with the driving field (dashed-dotted line).

TABLE I. Photon energy, corresponding excess energy relative to the minimum of the conduction band, and conduction-band valleys [the L valley is 0.3 eV above the Γ valley (Refs. 42 and 43)] that can be reached, for the different excitation wavelengths used.

Wavelength (nm)	Photon energy (eV)	Excess energy (eV)	Valley
885	1.40	≈ 0	Γ
800	1.55	0.11	Γ
750	1.65	0.20	Γ
680	1.82	0.36	Γ, L
650	1.91	0.43	Γ, L

it increases with delay. Exponential fits yield a rise time of 5 ps for 800 and 680 nm and a rise time of 14 ps for 650 nm. The rise time of 5 ps agrees very well with the time-resolved photoluminescence data of Ref. 44 (open circles).

IV. DISCUSSION

The THz field strength applied in our experiments is low enough to limit electron transport to the Γ valley of GaAs with a parabolic conduction band structure. THz-induced tunneling[47] is unimportant because of the high carrier temperatures and because of the comparably low driving fields used. All of the experimental results shown above are consistent with our picture of high-field THz transport in an electron-hole plasma from Sec. II.

As we have seen in Fig. 4, the transport is very sensitive to the frequency of the driving THz pulse. This is explained by the frequency dependence of the plasma heating by the THz radiation. In a THz field with a frequency of 3 THz, the electrons do not reach such high velocities as in a field with a frequency of 2 THz. Additionally, its velocity changes direction more frequently. According to Eq. (6), both of these effects result in a much smaller heating rate. As a consequence, the electrons in a 3-THz field never feel a significant friction force and, thus, move ballistically within the duration of the THz pulse.

One expects that the electron motion is always ballistic initially. This is the case for the measurements shown in Fig. 4 and in Figs. 1 and 2 of Ref. 10. However, this seems not to be always the case when the electrons are created within the driving THz pulse, as illustrated in Fig. 5. When the photoelectrons are created within the THz pulse, oscillations with a frequency of 4 THz are seen in both the emitted field's amplitude and ballisticity. The maxima in amplitude and ballisticity occur when the photoelectrons are injected at the extrema of the driving field, and the minima at the zero crossings of the driving field. The reason for this effect is that the electrons are created with an average velocity of zero. At the field extrema, ballistically moving electrons have velocity zero [Eq. (10)]. Therefore, electrons created at these times move in phase with the current expected for ballistic transport, leading to the observed maxima for the emitted field amplitude and the ballisticity. On the other hand, if the electrons are created when the driving field is zero and ballistic electrons have their maximum velocity, the newly created electrons have a velocity $\pi/2$ out of phase with ballistic transport.

To further illustrate this effect, we modified our theoretical model to account for the carrier injection at various phases of the THz pulse. Instead of modeling a time-dependent carrier density, we used a constant carrier density, but truncated the THz driving field with a smoothed step function in time centered at the moment of carrier injection:[48]

$$E_{\mathrm{dr}}(t,\tau) = \frac{E_{\mathrm{probe}}(t)}{2} \left[\mathrm{erf}\left(\frac{t+\tau}{\Delta t_{\mathrm{pump}}}\right) + 1 \right]. \qquad (12)$$

In the calculation we used the measured driving THz pulse at each delay. For the excitation pulse intensity, a 70-fs Gaussian pulse (which was its measured pulse duration) was used. To calculate the emitted THz field from the current, we used Eq. (8). The results are shown in Figs. 5(c) and 5(d). Our theory reproduces the measured oscillations along $t = -\tau$ very well.
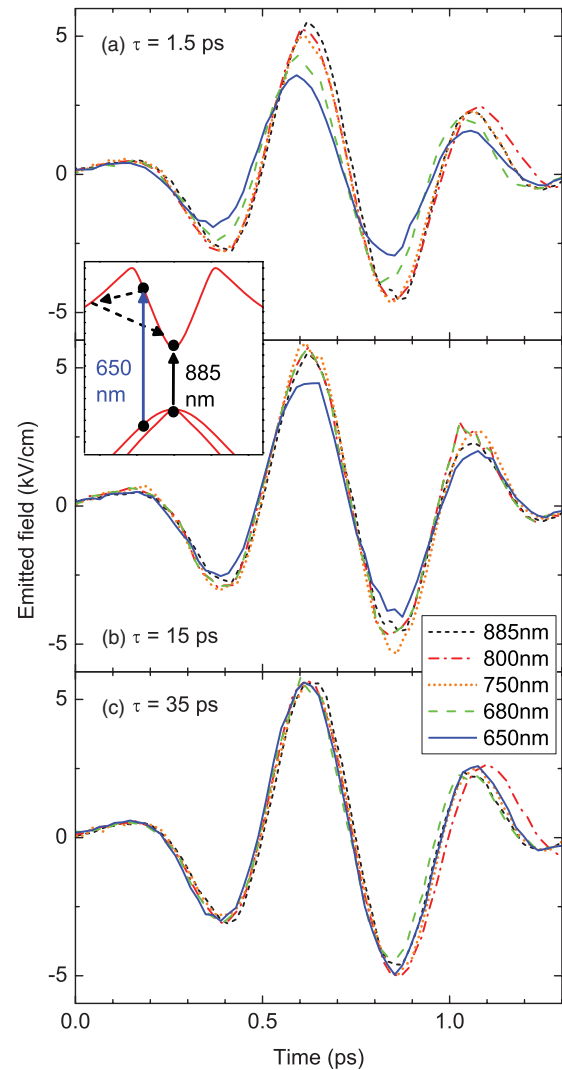

FIG. 7. (Color online) Measured emitted field of photoexcited carriers using several excitation wavelengths (as indicated) for delays τ between the excitation pulse and the THz pulse of (a) 1.5 ps, (b) 15 ps, and (c) 35 ps. The inset shows the electronic band structure of GaAs. For excitation wavelengths shorter than 700 nm, the electrons have enough energy to scatter into the L valley, from which they return to the Γ valley with a time constant (Ref. 44) of 5 ps.
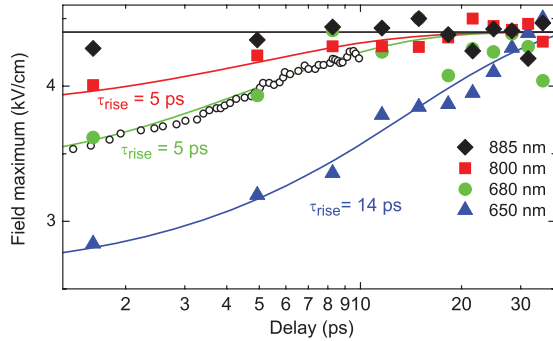
FIG. 8. (Color online) Symbols: amplitude of the emitted THz transient as a function of the delay τ for excitation wavelengths as indicated. Solid lines: exponential fits with τ_{rise} as indicated. Open circles: return of electrons to the Γ valley as measured in time-resolved photoluminescence [data are taken from the line in Fig. 2(b) of Ref. 44 and scaled to agree with our results at 2 ps].

With different excitation wavelengths we generate electrons at different points in the band structure. This nonthermal distribution thermalizes very quickly.[49] The distribution can then be described by a Boltzmann distribution function with an electron temperature higher than the lattice temperature. Subsequent cooling of the carriers is expected to be faster than 1 ps at room temperature, the temperature of our experiments.[49] Therefore, our transport measurements, independent of excitation wavelength, all start with a thermal carrier distribution at room temperature with an overall average velocity $\nu_e = 0$. We, however, find (Fig. 7) that the emitted fields for delays of 1.5 and 15 ps are different for different excitation wavelengths.

This dependence on excitation wavelength is caused by two effects. The first effect is a partial transfer of electrons to the side valleys immediately after photoexcitation of the electron-hole plasma. In GaAs, the minima of the L and X valleys[42,43] are 300 and 480 meV higher than that of the Γ valley. With excitation wavelengths shorter than ≈ 700 nm, the electrons have enough excess energy to scatter to the L valley. Since thermalization within the Γ valley[49] happens on a similar time scale as the transfer to the L and X valleys, we do not expect sharp thresholds for scattering into these side valleys. Thus, some scattering to the L valley can occur even at wavelengths of 800 nm. Since the electron mass in the side valleys is much higher, the electrons in the side valleys make only a negligible contribution to the current; they are essentially lost for transport.

Although scattering to the side valleys is known to happen very quickly (≈ 50 fs), it takes much longer for the electrons to return to the Γ valley.[44,50,51] In our measurements, the temporal resolution is limited by the half-cycle of the THz pulse (2507 fs), so we could not resolve the ultrafast transfer of electrons from the Γ valley to the side valleys. Their slow return to the Γ valley results in the slow increase of the emitted current shown in Fig. 8. This plot also contains exponential fits to the experimental data (solid lines). The gradual rise time $\tau_{\mathrm{rise}} = 5$ ps of the 800- and 680-nm data perfectly matches the return time of electrons to the Γ valley as measured in time-resolved photoluminescence[44] (open circles).
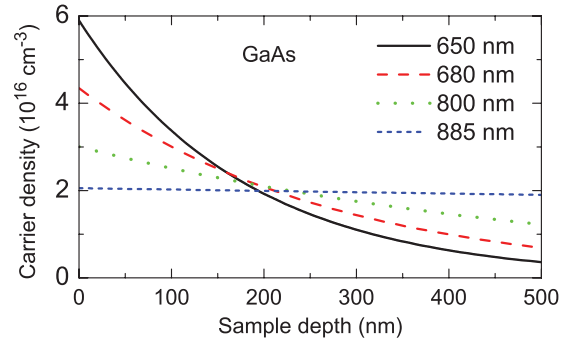

FIG. 9. (Color online) Initial carrier density versus sample depth for the different photoexcitation wavelengths.

At an excitation wavelength of 650 nm, another effect becomes important, namely, the inhomogeneous carrier density due to the short penetration depth of the excitation pulses into the GaAs layer (see Fig. 9). This results in a higher local carrier density close to the front surface of the GaAs layer and an increase of the momentum relaxation rates (cf. Fig. 1), additionally reducing the emitted THz amplitude. For longer excitation wavelengths such as 680 nm, this effect plays a minor role. The spatially inhomogeneous electron-hole plasma relaxes toward a homogeneous distribution of lower density via ambipolar diffusion,[52] that is, electrons and holes have to diffuse together. This results in ambipolar diffusion being much slower than the diffusion of electrons alone. In GaAs, the time constant for this ambipolar diffusion is 13 ps, which agrees very well with the observed rise time of the THz amplitude of 14 ps (Fig. 8).

At wavelengths shorter than 650 nm, the front AlGaAs layer of our sample begins to significantly absorb the excitation pulse. We measured the emitted fields also with 400-nm excitation (not shown here), where the AlGaAs absorbs all of the excitation photons. At short delays, this is essentially a measurement of the photoelectron transport in AlGaAs. In these data, the transport was ballistic initially, but the transition to driftlike motion was much faster than in GaAs. By the end of the driving THz pulse, the transport was nearly driftlike. We found that as we increased the delay between the excitation and the THz pulse, the transport did become more ballistic because the carriers slowly diffuse into the GaAs layer. Even after a 70-ps delay, the transport was still more driftlike than in GaAs, indicating that carriers remained in the AlGaAs layer.

V. CONCLUSIONS

Our THz experiments give evidence that the transport in an electron-hole plasma in a semiconductor is very different from transport by electrons and holes alone. In GaAs, the current from holes is much smaller than the current from the same density of electrons. The presence of holes leads, however, to an increase of scattering and thus to a faster transition from the initial ballistic transport to drift transport. If electrons and holes are generated with enough excess energy, a fraction of the electrons scatter into side valleys where they do not contribute to the current. Because of the increase of scattering with hole

density, a spatially inhomogeneous distribution carries less current than a homogeneous distribution.

For the theoretical description of these results, we have presented a model based on the description of carriers as spatially extended wave packets. The motion of these wave packets is governed by Ehrenfest's theorem, which results

in a decreased coupling to other elementary excitations with wavelengths comparable or less than the wave-packet size. The wave-packet size is changed by incoherent heating of the carriers. Another important point of the model is that the local field acting on the carriers is different from the incident field, caused by spatial correlations between the carriers.

---

[1] R. Ulbricht, E. Hendry, J. Shan, T. F. Heinz, and M. Bonn, Rev. Mod. Phys. **83**, 543 (2011).

[2] P. Gaal, W. Kuehn, K. Reimann, M. Woerner, T. Elsaesser, and R. Hey, Nature (London) **450**, 1210 (2007).

[3] W. Kuehn, P. Gaal, K. Reimann, M. Woerner, T. Elsaesser, and R. Hey, Phys. Rev. Lett. **104**, 146602 (2010).

[4] F. Blanchard, D. Golde, F. H. Su, L. Razzari, G. Sharma, R. Morandotti, T. Ozaki, M. Reid, M. Kira, S. W. Koch, and F. A. Hegmann, Phys. Rev. Lett. **107**, 107401 (2011).

[5] M. Woerner and T. Elsaesser, in *Dynamics at Solid State Surfaces and Interfaces*, Vol. 1, edited by U. Bovensiepen, H. Petek, and M. Wolf (Wiley-VCH, Weinheim, 2010), pp. 3–32.

[6] M. V. Fischetti, IEEE Trans. Electron Devices **38**, 634 (1991).

[7] A. Leitenstorfer, S. Hunsche, J. Shah, M. C. Nuss, and W. H. Knox, Phys. Rev. Lett. **82**, 5140 (1999).

[8] A. Leitenstorfer, S. Hunsche, J. Shah, M. C. Nuss, and W. H. Knox, Phys. Rev. B **61**, 16642 (2000).

[9] M. Abe, S. Madhavi, Y. Shimada, Y. Otsuka, K. Hirakawa, and K. Tomizawa, Appl. Phys. Lett. **81**, 679 (2002).

[10] P. Bowlan, W. Kuehn, K. Reimann, M. Woerner, T. Elsaesser, R. Hey, and C. Flytzanis, Phys. Rev. Lett. **107**, 256602 (2011).

[11] W. H. Zurek, Phys. Rev. D **24**, 1516 (1981).

[12] W. H. Zurek, Nature (London) **412**, 712 (2001).

[13] W. H. Zurek, Rev. Mod. Phys. **75**, 715 (2003).

[14] F. Rossi and C. Jacoboni, Semicond. Sci. Technol. **7**, B383 (1992).

[15] W. Magnus and W. Schoenmaker, Phys. Rev. B **47**, 1276 (1993).

[16] J. H. Collet, Phys. Rev. B **47**, 10279 (1993).

[17] H. Haug and A. P. Jauho, *Quantum Kinetics in Transport and Optics of Semiconductors* (Springer, Berlin, 1996).

[18] J. Shah, *Ultrafast Spectroscopy of Semiconductors and Semiconductor Nanostructures*, 2nd ed. (Springer, Berlin, 1999).

[19] D. S. Chemla and J. Shah, Nature (London) **411**, 549 (2001).

[20] F. Rossi and T. Kuhn, Rev. Mod. Phys. **74**, 895 (2002).

[21] V. M. Axt and T. Kuhn, Rep. Prog. Phys. **67**, 433 (2004).

[22] A. Kawabata, Rep. Prog. Phys. **70**, 219 (2007).

[23] S. T. Cundiff, Opt. Express **16**, 4639 (2008).

[24] E. Malic, T. Winzer, E. Bobkin, and A. Knorr, Phys. Rev. B **84**, 205406 (2011).

[25] G. D. Mahan, *Many-Particle Physics*, 3rd ed. (Kluwer, New York, 2000).

[26] In general, the dielectric function is a rank-two tensor, which can also depend on the direction of $\vec{q}$. However, since the holes do not contribute to the current, their distribution will remain centered around $q = 0$, leading to a scalar hole susceptibility depending only on the magnitude of $\vec{q}$. As the electron susceptibility does not contribute at all, Eq. (5), the dielectric function will be a scalar and will not depend on the direction of $\vec{q}$.

[27] N. Janssen and W. Zwerger, Phys. Rev. B **52**, 9406 (1995).

[28] A. F. J. Levi and Y. Yafet, Appl. Phys. Lett. **51**, 42 (1987).

[29] J. F. Young and P. J. Kelly, Phys. Rev. B **47**, 6316 (1993).

[30] M. Woerner and T. Elsaesser, Phys. Rev. B **51**, 17490 (1995).

[31] W. Bardyszewski, Solid State Commun. **57**, 873 (1986).

[32] T. Elsaesser, J. Shah, L. Rota, and P. Lugli, Phys. Rev. Lett. **66**, 1757 (1991).

[33] For excitation resonant to the band gap and for the present excitation density, hot-phonon effects are negligible.

[34] F. M. Peeters and J. T. Devreese, Phys. Rev. B **31**, 4890 (1985).

[35] Umklapp processes could change the total momentum, but because of the large momentum transfers q involved (the Coulomb scattering matrix element is proportional to $1/q^2$), they do not play a significant role.

[36] This lattice is independent of the crystal lattice of GaAs.

[37] O. F. Mossotti, Mem. Matem. Sci. Fis. Nat. Soc. Ital. Sci. **24**, 49 (1850).

[38] H. A. Lorentz, Wiedemanns Ann. **9**, 641 (1880).

[39] L. Lorenz, Wiedemanns Ann. **11**, 70 (1881).

[40] N. Wiser, Phys. Rev. **129**, 62 (1963).

[41] The reason that we use an ellipsoid is that there a uniform polarization leads to a uniform electric field (Ref. 53).

[42] D. E. Aspnes, C. G. Olson, and D. W. Lynch, Phys. Rev. Lett. **37**, 766 (1976).

[43] I. Vurgaftman, J. R. Meyer, and L. R. Ram-Mohan, J. Appl. Phys. **89**, 5815 (2001).

[44] J. Shah, B. Deveaud, T. C. Damen, W. T. Tsang, A. C. Gossard, and P. Lugli, Phys. Rev. Lett. **59**, 2222 (1987).

[45] T. Stroucken, A. Knorr, P. Thomas, and S. W. Koch, Phys. Rev. B **53**, 2026 (1996).

[46] K. Reimann, Rep. Prog. Phys. **70**, 1597 (2007).

[47] W. Kuehn, P. Gaal, K. Reimann, M. Woerner, T. Elsaesser, and R. Hey, Phys. Rev. B **82**, 075204 (2010).

[48] I. Babushkin, W. Kuehn, C. Köhler, S. Skupin, L. Bergé, K. Reimann, M. Woerner, J. Herrmann, and T. Elsaesser, Phys. Rev. Lett. **105**, 053903 (2010).

[49] T. Elsaesser and M. Woerner, Phys. Rep. **321**, 253 (1999).

[50] J.-Y. Bigot, M. T. Portella, R. W. Schoenlein, J. E. Cunningham, and C. V. Shank, Phys. Rev. Lett. **65**, 3429 (1990).

[51] P. C. Becker, H. L. Fragnito, C. H. B. Cruz, J. Shah, R. L. Fork, J. E. Cunningham, J. E. Henry, and C. V. Shank, Appl. Phys. Lett. **53**, 2089 (1988).

[52] K. Seeger, *Semiconductor Physics*, 5th ed. (Springer, Berlin, 1991).

[53] C. Kittel, *Introduction to Solid State Physics*, 7th ed. (Wiley, New York, 1996).